"Sticky" Hard Spheres: Equation of State, Phase Diagram, and Metastable Gels

Stefano Buzzaccaro, Roberto Rusconi, and Roberto Piazza*

Dipartimento di Ingegneria Nucleare, CSGI - Politecnico di Milano, via Ponzio 34/3, 20133 Milano (Italy)

(Received 17 May 2007; published 27 August 2007)

A large variety of engaging phenomena, ranging from crystallization in protein solutions to the formation of colloidal gels and glasses via depletion forces, stems from the occurrence of very short-ranged attractive forces. From depolarized light scattering measurements of equilibrium sedimentation profiles, we obtain an accurate description of the equation of state and of the phase diagram of colloids where depletion forces are tuned by the addition of a surfactant. For weak depletion, a colloidal fluid fully described by Baxter's "sticky" hard sphere model coexists with ultradense colloidal crystals. For stronger attractive interactions, kinetically arrested looser gels form, showing an elastic modulus that scales as a power law of the local particle concentration.

DOI: 10.1103/PhysRevLett.99.098301 PACS numbers: 82.70.Uv, 05.70.Ce, 47.57.ef, 82.70.Gg

The investigation of systems of colloidal particles interacting via very short-ranged attractive forces has yielded valuable and often unforeseen insights on the contingency of the liquid state and on the origin of metastable gel or glassy phases [1–4]. In this regard, the adhesive hard spheres (AHS) limit [5], corresponding to an attractive potential of vanishing range $u(r)/k_BT = -\ln[\sigma\delta(r-\sigma)/12\tau]$, where σ is the particle diameter and τ is a "stickiness parameter," has become the paragon model in the investigation of many topics, such as crystallization and competitive adsorption of proteins [6,7], percolation in microemulsions [8], even flocculation and renneting in dairy practice [9]. Yet, to what extent real systems *quantitatively* conform to the simple AHS model is often scarcely scrutinized. In addition, very short-ranged attractive forces beget fascinating effects, such as spontaneous finite-size clustering [10,11], calling for a rigorous investigation of AHS thermodynamics. Short range interactions due to depletion effects are commonly induced by adding to a colloidal suspension nonadsorbing polymers. An alternative route consists in using as a depletion agent the micellar aggregates spontaneously formed by a surfactant additive [12]. In this work, we plan to show that the study of the equilibrium sedimentation profiles of colloids with added nonionic surfactant offers an excellent opportunity to obtain, for the first time and with high resolution, the full equation of state of a system of AHS, to inspect fine details of the phase diagram, and to provide quantitative information on the structure and elastic properties of gel phases.

The approach we have followed fully exploits the unique material and optical properties of perfluorinated polymer colloids. The intrinsic optical anisotropy of these particles yields indeed a depolarized component in the light scattered by the suspension, which is an accurate probe of the local particle density [13]. Measurements of the inhomogeneous colloid concentration profile induced by an external field such as gravity is then a straightforward route to obtain the system equation of state and phase diagram [14]. As a further bonus, perfluorinated colloids have a high material density and do not swell in common solvents, allowing to obtain accurate values of the volume fraction Φ of the dispersed particles.

We have studied aqueous suspensions of spherical colloids, with a radius $R = 82 \pm 3$ nm, made of MFA, a perfluoromethoxy resin obtained by copolymerization of tetrafluoroethylene and perfluoromethylvinylether. As depletant, we have used the nonionic surfactant Triton X100, which at room temperature forms globular micelles with a radius $r \simeq 3$–4 nm, corresponding to size ratio $q = r/R \simeq 0.035$–0.05. The surfactant, which at very low concentration first adsorbs on the particle surface forming a compact monolayer [13], acts at the same time as a steric stabilizer. Suspensions were prepared at a fixed particle volume fraction $\Phi = 0.20$, in the presence of about 0.1 M NaCl to screen electrostatic interactions, and of a Triton volume fraction Φ_s in the solvent varying between 0 and 0.12. The samples were added of different amounts of urea to fully suppress coherent polarized scattering at $\lambda = 633$ nm by matching the solvent and particle refractive indices [13]. Depending on the amount of added Triton, the samples display two radically different kinds of behavior. When observed with natural light (where index matching is not perfect) samples with $\Phi_s \geq 0.082$ showed a sudden increase of turbidity, witnessing strong fluctuations of concentration, followed by rapid settling at a speed much larger than the Stokes velocity $v_S = 2\Delta\rho g R^2/9\eta$ ($\simeq 1.2$ mm/day), where $\Delta\rho$ is the density difference between MFA and the matching fluid, and $\eta \sim 1$ cP is the solvent viscosity. Conversely, suspensions with $\Phi_s \leq 0.07$ remained fully transparent and sedimented very slowly. All suspensions were then let settling and equilibrate for 170 days, corresponding to more than $10h/v_S$, where h is the sample height. Measurements of the equilibrium sedimentation profiles consist in detecting the depolarized scattered intensity I_{VH} as a function of the distance z from the sample bottom by vertically translating the cell, using the intensity scattered by the original homogeneous suspension for calibration. I_{VH} measurements allowed to ob-

tain accurate sedimentation profiles with a spatial resolution of about 50 μm in a volume fraction range covering almost four decades.

Equations of state.—All sedimentation profiles obtained for $\Phi_s \leq 0.082$ display a discontinuous jump to a lower denser phase S, separated from the upper phase by a sharp meniscus. While for samples with $\Phi_s \leq 0.027$ the particle concentration in S is close to the value expected for a colloidal crystal of hard spheres (HS), the denser phases obtained for $0.060 \leq \Phi_s \leq 0.082$ have a particle volume fraction which exceeds the random close packing value $\Phi_{\rm rcp} \simeq 0.64$ and continuously approaches the value for maximum ordered packing $\Phi_{\rm ocp} = \pi/3\sqrt{2} \simeq 0.74$. Although, due to the small particle size, we have no direct ways of checking for Bragg diffraction, we must therefore conclude that these structures must be at least partly (and, close to the cell bottom, almost fully) ordered. These almost close-packed structures, standing among the densest colloidal phases so far reported, display an extremely high mechanical strength to the point that they cannot be mechanically remixed, and they keep their concentration profile unmodified even when left standing upside down for a few days. They are nonetheless fully reversible: if the supernatant fluid is replaced with pure water, they spontaneously dissolve in less than 1 day. Notice that, even for $\Phi_s = 0.082$, the earliest fast-sedimenting fluid eventually restructures into a phase with $\Phi > \Phi_{\rm rcp}$. Conversely, for $\Phi_s > 0.082$ much looser phases are obtained, which will be discussed in the next section.

At low particle concentration, all profiles satisfy the usual barometric law $\Phi(z) = \Phi_0 \exp(-z/\ell_g)$, with closely matched gravitational lengths $\ell_g = 0.21 \pm 0.01$ mm that are slightly larger than the calculated value $\ell_g^{\rm th} = k_B T/\Delta\rho g v_p$ ($\simeq 0.17$ mm), where v_p is the particle volume. A very plausible explanation for this discrepancy, supported both by sedimentation velocity data and by measurements of the Φ dependence of the suspension refractive index, is that the particle density could be about 20% smaller than the bulk value for MFA [15].

A numerical integration of the particle volume fraction profile $\Phi(z)$ directly yields the local osmotic pressure

$$\Pi(z) = \Delta\rho g \int_z^h \Phi(z) dz, \qquad (1)$$

and therefore the full equations of state, which are displayed in Fig. 1 in terms of the compressibility factor $Z(\Phi) = (v_p/\Phi k_B T)\Pi(\Phi)$. In the absence of Triton (sample A), the experimental data are very well fitted by the Carnahan-Starling (CS) equation of the state in the fluid branch [17], and by $Z_{\rm HS}^{cc}(\Phi) = 3(1 - \Phi/\Phi_{\rm ocp})^{-1}$ in the lower phase, a mean-field expression which well approximates the numerical results for a HS colloidal crystal [18]. Notice that, once ℓ_g is fixed, no "adjustment" in Φ is required to match the theoretical concentrations of the coexisting HS phases. In the presence of the depletant

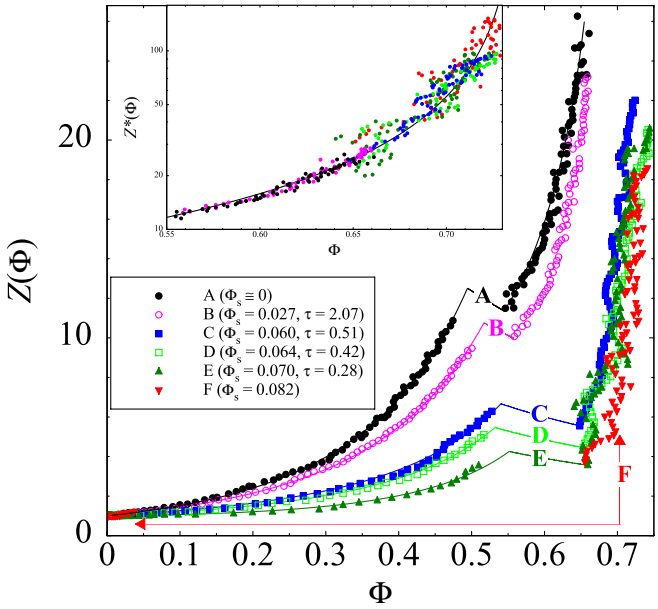

FIG. 1 (color online). Equations of state obtained from the equilibrium sedimentation profiles. The fluid branches are fitted using the CS expression for sample A and with the equation of state for AHS obtained via the "energy route" for samples B–E. For sample F, the fluid region is too limited to yield a meaningful value of τ. Inset: rescaling of the compressibility factors for the S branches as $Z^*(\Phi) = Z(\Phi)/\alpha(\tau)$.

(samples B–E), we have fitted the compressibility factor of the upper phases using the analytic equation of state for AHS derived via the "energy route," which is expected to yield accurate values for the stickiness parameter τ in the limit of weak adhesion [19]. Figure 1 shows that the AHS model describes extremely well all fluid branches, with fitted values for τ covering the range $0.2 \lesssim \tau \lesssim 2$. However, at variance with the close-packed, ideally incompressible AHS crystal, all solid phases show a *finite* compressibility. The inset of Fig. 1 suggests that all $Z(\Phi)$ can be rescaled on a single master curve by assuming $Z(\Phi) = 3\alpha(\tau)(1 - \Phi/\Phi_{\rm ocp})^{-1}$, where the scaling factor α decreases roughly linearly from $\alpha \simeq 0.8$ (sample B) to $\alpha \simeq 0.1$ (sample F). This amounts to say that $Z(\Phi)$ is reduced from the value for a HS crystal by an "energy" factor that increases with the strength of the attractive interactions and weakly depends on Φ.

Phase diagram.—To inquire whether interpreting the equation of state in terms of the AHS model is consistent, we first relate the measured values of τ to the concentration of the depletant by matching to the AHS model the second virial coefficient B_2 of the standard Asakura-Oosawa depletion potential [4,20], which, for $q \ll 1$ and assuming noninteracting surfactant micelles, can be written as $U_{\rm AO}(x) \simeq -3k_B T\Phi_s(1 - x)^2/2q$, where, in terms of the interparticle distance d, $x = (d - 2R)/2Rq$. A numerical fit to our data, shown in the inset in Fig. 2, yields $q \simeq 0.022$, which is slightly smaller than the lower calculated

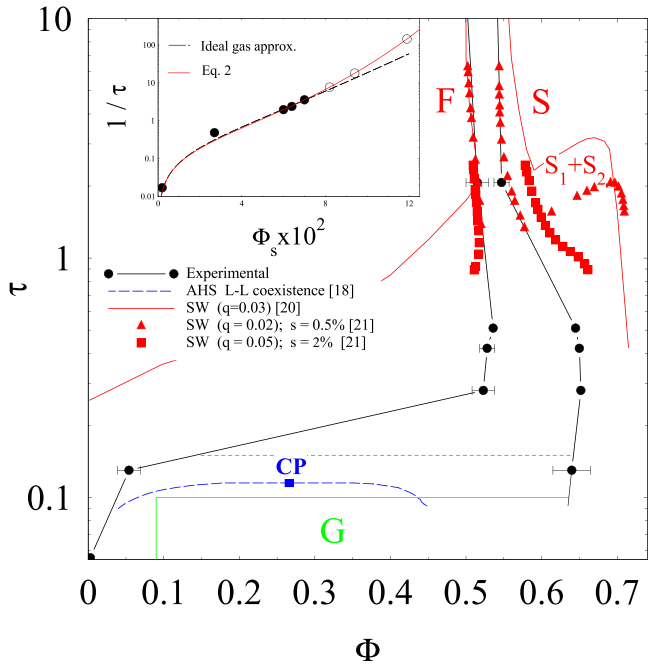

FIG. 2 (color online). Inset: dependence on surfactant concentration of the τ values obtained from the equations of state (●), with numerical fits and extrapolated τ values for samples F, G, and H (○). Body: experimental phase diagram (●) compared to the theoretical predictions for a square-well (SW) potential with $q = 0.03$ [21], and to numerical simulations for the same potential, but with finite particle polydispersity [22], for different values of q and polidispersity index s. The AHS fluid-fluid coexistence curve is plotted according to [19]. In region G long-living gels form, while the dotted line marks the lowest value of Φ_s where transient aggregation is observed.

bound for the size ratio. It is, however, useful to investigate how intermicellar interactions may modify this picture. The nonideality of the surfactant can be accounted for by recalling that, for small q and moderate concentration of weakly interacting small spheres, the depletion potential can be approximated by the product of the excluded volume times the osmotic pressure of the depletant [2]. A simple calculation then yields:

$$\tau^{-1} = 12q \int_0^1 dx(1+qx)^2[e^{3\Phi_s Z_s(\Phi_s)(1-x)^2/2q} - 1], \quad (2)$$

where $Z_s(\Phi_s)$ is the compressibility factor of the surfactant solution. The latter can be directly obtained from light scattering measurements of the osmotic compressibility of Triton solutions yielding, for $0 < \Phi_s \lesssim 0.2$, $Z_s(\Phi_s) \simeq 1 - 0.12\Phi_s + 19\Phi_s^2$. Notice that, even if B_2 is very small, higher order interaction terms *cannot* be neglected for $\Phi_s \simeq 0.1$. The full line in the inset (corresponding to a best-fit value $q \simeq 0.025$) shows that the ideal-gas approximation tends to overestimate τ for $\Phi_s \gtrsim 0.07$. We have then used Eq. (2) to extrapolate the value of τ for samples F ($\Phi_s = 0.082$, $\tau = 0.13$), G ($\Phi_s = 0.094$, $\tau = 0.092$), and H ($\Phi_s = 0.119$, $\tau = 0.056$) (the latter two yielding gel phases we shall later discuss).

The experimental values for the phase boundaries are compared in Fig. 2 to the theoretical prediction for a square-well potential with $q = 0.03$ obtained by Foffi *et al.* [21] (once again mapped on a τ axis by virial coefficient matching). We may first of all notice that the experimental fluid-solid coexistence region is much narrower than theoretically predicted. In particular, the volume fraction of the S phases at coexistence is consistently smaller than expected. Moreover, while theory predicts the coexistence of two isostructural solids ($S_1 + S_2$) at high Φ, we have found no evidence of a solid-solid equilibrium. These discrepancies are very likely due to polydispersity effects. Numerical simulation results by Bolhuis and Frenkel [22], displayed in Fig. 2, show indeed that a polydispersity index as low as $s = 0.01$ fully quenches the isostructural transition and noticeably narrows the coexistence region. We nonetheless regard as interesting that a polydisperse AHS crystal displays a compressibility factor so much akin to Z_{HS}^{cc}. Finally, close to the HS limit, the freezing line shows a negative slope. In other words (as already apparent in Fig. 1), the limiting fluid density first *increases* with Φ_s, yielding a slightly reentrant shape of the freezing line as predicted in [21,22].

Transient effects and long-living gels.—The upper inset of Fig. 3 summarizes the very peculiar sedimentation kinetics observed for sample F. Just after mixing, a moderately concentrated phase forms and settles with a sedimentation velocity $v \sim 10^3 v_S$. However, after a few

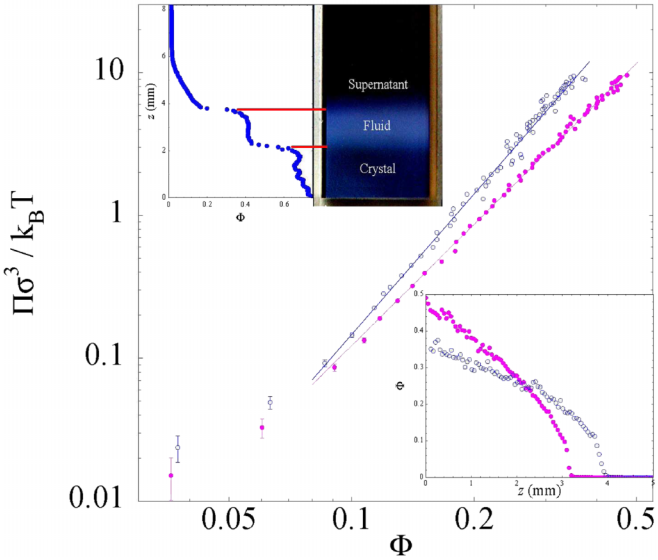

FIG. 3 (color online). Upper inset: sedimentation profile for sample F, with a (contrast-enhanced) image of the sedimentation cell, obtained 30 minutes after mixing. Lower inset: stationary sedimentation profiles for samples G (●) and H (○). Body: osmotic pressure of the same gels, normalized to $k_B T/\sigma^3 \simeq 0.92$ Pa, where σ is the particle diameter.

minutes, a second meniscus, separating the sedimenting suspension from a less turbid lower phase, becomes evident close to the cell bottom. By gently tilting the cell, the upper meniscus (but not the lower) keeps horizontal, showing that the fast-sedimenting phase has no finite yield modulus. Eventually, the sediment is made of a single concentrated phase with $\Phi > \Phi_{\mathrm{rcp}}$. This transient behavior was found to be fully reproducible for additional samples with a Triton concentration in the narrow range $0.080 \lesssim \Phi_s \lesssim 0.085$, corresponding to $0.10 \lesssim \tau \lesssim 0.15$. Figure 2 shows that the extrapolated τ value for sample F is just slightly larger than the value $\tau_c \simeq 0.11$ corresponding to the critical point for AHS. It is therefore tempting to assume that the upper phase is made of finite-size aggregates, and that this transient aggregation is driven by the proximity of the liquid-liquid coexistence curve.

For larger values of Φ_s substantially ''expanded'' sedimentation profiles are attained on a time scale of a few days, and they keep essentially unchanged for more than 6 months. These structures show clear evidence of kinetic arrest, such as a totally frozen scattering speckle pattern and a noticeable yield modulus, and they should then be regarded as disordered ''gels.'' Since samples G and H lie well inside the metastable fluid-fluid coexistence curve in Fig. 2, their rapid sedimentation process can then presumably be envisaged as a liquid-liquid phase separation followed by structural arrest. The metastable nature of these phases is highlighted by a simple experiment. If the supernatant fluid of a sample settled by more than one month is modified, so to reduce Φ_s from 0.12 to 0.07, the gel restructures on a time scale of *a few hours* into a new phase with a concentration profile resembling the AHS crystals obtained by slow sedimentation.

For a gel-like structure, it is tempting to interpret $\Pi(\Phi)$ in Eq. (1) as the local compressive elastic modulus. Physically, this amounts to state that the colloid concentration at a given height z increases until reaching the value needed to sustain the weight of the particles laying above. Figure 3 shows that, for both samples G and H, $\Pi(\Phi)$ behaves as Φ^m, with an exponent $m \simeq 2.8$–3 which slightly increases with Φ_s. For both profiles, the power-law behavior extends down to particle volume fractions $\Phi \simeq 0.1$. A power-law behavior of the compressive yield stress versus particle concentration has already been observed, by pressure filtration and centrifugation measurements, for flocculated colloidal suspensions [23], and it has been numerically predicted for polymer-depletion gels [24]. Interpreting $\Pi(\Phi)$ as an elastic modulus is, however, meaningful only provided that solid friction effects are negligible. This does not hold true for dilute irreversible colloidal gels [25], where a noticeable horizontal component of the stress is sustained by the cell walls, so that a given section of the gel effectively bears only the weight of a finite slice laying above. As a result of friction, the gel structure should display a rather complex dependence on cell geometry and initial particle volume fraction. Yet test measurements we are currently performing do not seem to evidence similar effects. Likely, wall friction plays then a lesser role for highly concentrated depletion gels than for tenuous irreversible gels. Our results therefore suggest that sedimentation data can be an accurate probe of the elastic properties and of the ageing of colloidal gels.

We thank Solvay-Solexis for having provided us the Hyflon™ MFA particle batch and P. Charbonneau, L. Cipelletti, V. Degiorgio, M. Dijkstra, R. Evans, A. Fortini, and D. Frenkel for useful suggestions and comments.

*roberto.piazza@polimi.it

[1] W. C. K. Poon, Science **304**, 830 (2004).
[2] R. Roth, R. Evans, and L. L. Louis, Phys. Rev. E **64**, 051202 (2001).
[3] P. Charbonneau and D. R. Reichman, Phys. Rev. E **75**, 011507 (2007).
[4] M. Dijkstra, J. M. Brader, and R. Evans, J. Phys. Condens. Matter **11**, 10 079 (1999).
[5] G. Stell, J. Stat. Phys. **63**, 1203 (1991).
[6] R. Piazza, Curr. Opin. Colloid Interface Sci. **5**, 38 (2000).
[7] E. Dickinson, J. Chem. Soc., Faraday Trans. **88**, 3561 (1992).
[8] S. H. Chen, J. Rouch, F. Sciortino, and P. Tartaglia, J. Phys. Condens. Matter **6**, 10 855 (1994).
[9] C. G. de Kruif, J. Colloid Interface Sci. **185**, 19 (1997).
[10] H. Sedgwick *et al.*, Eur. Phys. J. E **16**, 77 (2005).
[11] P. J. Lu *et al.*, Phys. Rev. Lett. **96**, 028306 (2006).
[12] R. Piazza and G. Di Pietro, Europhys. Lett. **28**, 445 (1994).
[13] V. Degiorgio, R. Piazza, T. Bellini, and M. Visca, Adv. Colloid Interface Sci. **48**, 61 (1994).
[14] R. Piazza, T. Bellini, and V. Degiorgio, Phys. Rev. Lett. **71**, 4267 (1993).
[15] In addition, we did not detect *any* dependence of ℓ_g on initial particle concentration or sediment height. This fully ''regular'' behavior of ℓ_g, which is consistent with the results of Ref. [16] but contrasts with the evidences reported in [14], will be thoroughly discussed in a forthcoming paper dealing with sedimentation dynamics.
[16] C. P. Royall, R. van Roij, and A. van Blaaderen, J. Phys. Condens. Matter **17**, 2315 (2005).
[17] N. F. Carnahan and K. E. Starling, J. Chem. Phys. **51**, 635 (1969).
[18] K. R. Hall, J. Chem. Phys. **57**, 2252 (1972).
[19] M. A. Miller and D. Frenkel, J. Chem. Phys. **121**, 535 (2004).
[20] S. Asakura and F. Oosawa, J. Chem. Phys. **22**, 1255 (1954).
[21] G. Foffi *et al.*, Phys. Rev. E **65**, 031407 (2002).
[22] P. Bolhuis, Ph.D. thesis, Utrecht University, 1996.
[23] J. J. Guo and J. A. Lewis, J. Am. Ceram. Soc. **82**, 2345 (1999).
[24] V. Kobelev and K. S. Schweizer, J. Chem. Phys. **123**, 164902 (2005).
[25] J.-M. Condre, C. Ligoure, and L. Cipelletti, J. Stat. Mech. (2007) P02010.